An Array of Ferromagnetic Nanoislands Nondestructively Patterned *via* a Local Phase Transformation by Low-Energy Proton Irradiation

Sanghoon Kim, Soogil Lee, and Jongill Hong*

Materials Science and Engineering, Yonsei University, Seoul 120-749, Korea

ABSTRACT Low-energy proton irradiation was applied to pattern an array of metallic, ferromagnetic nanoislands through the local phase transformation of an oxidic, paramagnetic phase in a complex superlattice composed of repetitions of an oxidic and metallic layer. The irradiation inflicted minimal damage on the structure, resulting in the absence of unwanted defects and side effects. This nondestructive pattern transfer was clearly confirmed by the contrast between irradiated and unirradiated regions in electrical, chemical, and magnetic images. Simulation based on the magnetic properties suggests that this low-energy proton irradiation can nondestructively pattern an array of ferromagnetic islands with 8.2 nm in diameter and 7.4 nm in spacing between islands, which means it can achieve an areal density of ~3 Tb/in.^{2} with a thermal stability of over 80 k_BT. Such an array is strong enough to overcome the so-called superparamagnetism limit in magnetic recording. The attributes demonstrated here corroborate that proton irradiation can be applied to design and pattern devices on a nanometer scale not only for magnetic but also for electric and optical materials systems in all such systems in which a local phase transformation is available.

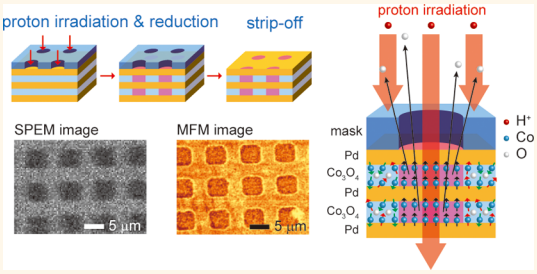

KEYWORDS: proton irradiation · phase transformation · nanopattering · ferromagnetic nanoisland

The demand for increased storage capacity in magnetic recording is higher than ever. It has been partly addressed by the rapid development of high-density magnetic media meant to counter the imminent threat of competitors, such as solid-state memories, appearing on the market.[1,2] Nanoscale magnetic patterning without substantial side effects holds the key to radically increasing the capacity not only of magnetic recording storage but of magnetic memories, spin-logic, and spin-quantum computing devices,[3−10] as well as to designing new spintronic devices.[11−13] Among methods of nanopatterning, ion irradiation is particularly promising for the development of high-density devices of several terabits per square inch (Tb/in.^{2}) since it has significant advantages over conventional methods. For example, it does not require a number of complicated fabrication steps such as physical or chemical etching, nonmagnetic materials filling, and planarization to create an array of ferromagnetic islands. Ion irradiation can thereby avoid the lethal side effects of conventional patterning, in particular for a few nm-thick pillar patterns. Various ferromagnetic metallic systems, such as Co/Pt, Co/Pd, CoCrPt/Cr superlattices, FeAl, and $CrPt_3$, with ion sources such as He, Ar, Ga, and Xe in the energy range of 10s keV ~ 10s MeV have been explored with successful results in magnetic nanopatterning.[14−22] Local destruction of an interfacial structure or a crystal structure in an atomic short-range-order by bombardment with accelerated ions has been a fundamental mechanism to achieve such patterning. However, unavoidable drawbacks of this method are (1) unwanted defect formations due to high energy or heavy ion bombardments;[15,16,20,21] (2) cross-talk or exchange coupling between patterns through the unpatterned ferromagnetic medium,[22] which results in a loss of control over magnetic switching; and (3)

* Address correspondence to hong.jongill@yonsei.ac.kr.

Received for review January 22, 2014 and accepted April 22, 2014.

Published online April 22, 2014
10.1021/nn500683b

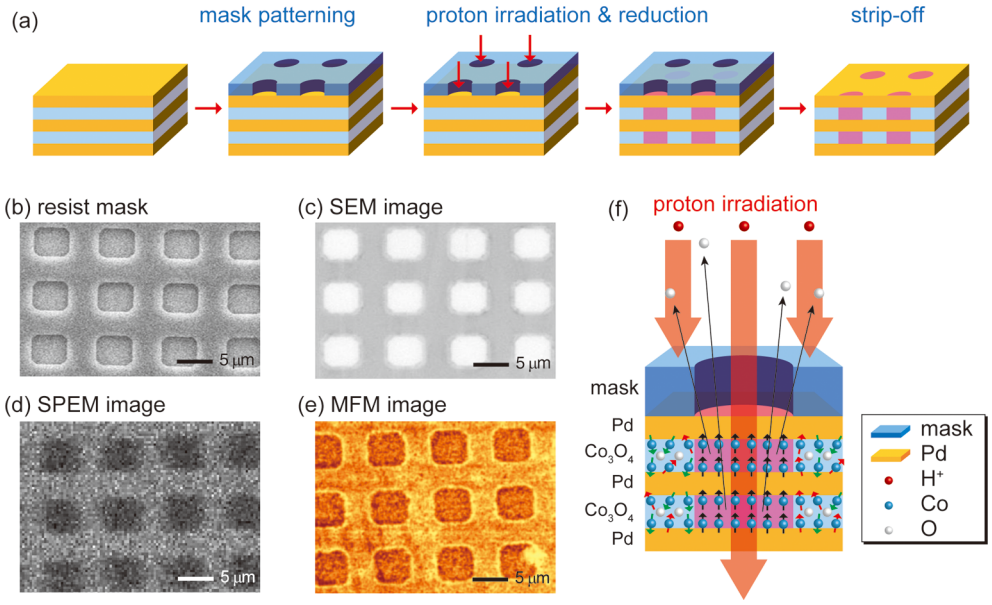

Figure 1. (a) A schematic diagram of the patterning process. SEM images of a photoresist square array of 5 μm $\times$ 5 μm after irradiation before (b) and after (c) removal of the resist. The secondary electrons contrast oxidic (masked and unirradiated) and metallic (unmasked and irradiated squares) regions. (d) SPEM oxygen mapping using the O 1s spectrum reveals oxygen-rich (bright) and oxygen-free (dark) regions. (e) MFM indicates that the magnetic patterns are in a single domain state with PMA. (f) Illustration of the nanoscale patterning by the proton irradiation.

limitations in the use of various material systems such as oxides, nitrides, and sulfides. Proton irradiation with low energy (far below 1 keV) has been suggested to solve those problems because the proton, being the lightest and smallest ion, has a bombardment energy that is small enough to ensure minimal damage to the physical and chemical structures of the materials to be patterned.[23] Proton irradiation with 0.3 keV has indeed succeeded in local phase transformation from an *oxidic, paramagnetic* Co_3O_4/Pd to a *metallic, ferromagnetic* Co/Pd superlattice without any noticeable damages. This alternate methodology of nanopatterning is unlike any of the other irradiation methods.[24]

In this study, we demonstrate that an array of ferromagnetic nanoislands patterned by the local phase transformation of a Co_3O_4/Pd superlattice with proton irradiation is of sufficiently high quality to signal a major breakthrough in the field of magnetic data storage. Our simulation based on experimental results estimates a pitch of ~15 nm in patterning resolution, which corresponds to a bit patterned media (BPM) with magnetic-recording density of 3 Tb/in.^{2}. For reference, the current magnetic-recording density is under 1 Tb/in.^{2}. In addition, our irradiation method has the distinct advantages of (1) the absence of the need to flatten a surface or fill the gaps between patterns; (2) flexibility in the use of various material systems such as metals, oxides, nitrides, and sulfides; (3) the lack of exchange coupling or cross-talk among ferromagnetic patterns; and (4) well-preserved interfaces of the phase transformed Co/Pd superlattice that are sufficiently intact to induce interfacial perpendicular magnetic anisotropy (PMA) stronger than that of the metallic superlattice prepared for reference. All of these advantages solve the fatal predicaments encountered by current BPM technology. The PMA of our individual nanoislands is strong enough to overcome superparamagnetism.

RESULTS AND DISCUSSION

Figure 1a illustrates how the array of ferromagnetic nanoislands was patterned by the proton irradiation: (1) photoresist mask patterns generated by e-beam lithography, (2) the proton irradiation, (3) removal of photoresist, and (4) resulting magnetic patterns. At first, we made the array with a pattern size of 5 μm $\times$ 5 μm using proton irradiation at a dose of 1.48 $\times$ 10^{17} ions/cm^2 in order to investigate the chemical uniformity of patterns by a scanning photoelectron microscope (SPEM). For reference, our spatial resolution of our SPEM was ~2 μm. The proton dose of 1.48 $\times$ 10^{17} ions/cm^2 was confirmed to transform the paramagnetic oxidic phase to ferromagnetic metallic nanoislands and was kept constant except where otherwise mentioned in this article. Because the secondary electron population in the masked (or oxidic) regions is much smaller than that in the unmasked (or reduced metallic) regions, the scanning electron microscopy (SEM) image clearly contrasts the patterns from the medium background, as shown in Figure 1c. SPEM using an oxygen 1s spectrum shows that the dark squares in Figure 1d correspond to oxygen-free areas; *i.e.*, they became reduced and metallic. The bright background indicates oxygen-rich regions. The SPEM image reveals that the patterns are chemically well-defined. The magnetic force microscopic (MFM)

image (Figure 1e), too, reveals a successful magnetic patterning by showing that the proton-irradiated region has indeed turned ferromagnetic, unlike the other paramagnetic areas. The patterns were magnetically saturated with PMA after a field larger than 0.4 T was applied. Because all three images—electrical, chemical, and magnetic—were consistent with one another, they are direct evidence of successful magnetic patterning *via* two simultaneous transformations of chemical and magnetic phases by the proton irradiation. The chemical-transformation or reduction induced by the proton irradiation is explained as follows: When protons are irradiated onto the Co_3O_4/Pd superlattice at an energy of 0.5 keV, they transfer their kinetic energy to atoms in the superlattice. When this transfer energy (E_t) is larger than the displacement energy (E_d) of an atom, the atom may be displaced or removed from its position, leaving behind a vacancy. Among the elements in the superlattice, oxygen is the most likely one to be removed because the maximum E_t is much larger than oxygen's E_d at 0.5 keV irradiation. According to the classical two-body collision model,[25] the E_t from the proton to the oxygen is estimated to be 112.0 eV, which is about nine times higher than oxygen's E_d of 12.5 eV.[23] In contrast, the E_t vlaues of Co, Pd, and Ta atoms are much lower than their E_ds, resulting in no effect on the displacements.[26] As a result, only oxygen is displaced and diffused out to vacuum, as illustrated in Figure 1f, resulting in the simultaneous phase transformation from oxidic and paramagnetic Co_3O_4 to metallic and ferromagnetic Co in the Co_3O_4/Pd superlattice during the proton irradiation. As a matter of fact, our simulation using Stopping and Range of Ions in Matter (SRIM) open-source software[27] estimates that the number of oxygen vacancies generated by the accelerated protons with 500 eV is more than that of oxygen atoms in the oxidic Co_3O_4/Pd superlattice: $\sim 2.8 \times 10^{16}$ vacancies *vs* $\sim 1.8 \times 10^{16}$ atoms. In other words, very few oxygen atoms remain after the proton irradiation. This estimation supports our postulated reduction mechanism.

It has been reported that hydrogen atoms affect magnetism in matter. For example, hydrogen-mediated magnetic ordering can be induced in ZnO or graphite after hydrogen treatment.[28,29] To investigate the hydrogen effect on the magnetism of the superlattices, we compared the magnetic properties of the metallic reference superlattice before and after the proton irradiation. The metallic Co/Pd superlattice with a structure similar to that of the reduced Co/Pd superlattice was irradiated under the same condition we used for the patterning. Magnetic properties of the metallic, the irradiated metallic, and the reduced Co/Pd superlattice films are listed in Table 1. The saturation magnetization (M_s) and PMA of the Co/Pd superlattice were decreased after the proton irradiation by ~15% and ~13%, respectively. Decrease in M_s and PMA of a hydrogenated Co/Pd superlattice can be attributed to the electron transfer from hydrogen atoms to Pd atoms or to changes in the electronic structure at the interface of the Co/Pd superlattice.[30,31] Hydrogenation of the Co layer can also be considered responsible for the decrease in M_s. According to theoretical work,[32] the M_s of CoH is smaller than that of Co by ~27%, meaning that the formation of a CoH phase may take place but is not dominant in either irradiated metallic or reduced Co/Pd superlattices. On the contrary, the reduced superlattice showed PMA larger than, but M_s smaller than, those of the metallic reference Co/Pd superlattice. In the case of the reduced superlattice, we believe that the magnetoelastic effect due to pseudomorphic growth is strong enough to overcome the negative effect of the hydrogenation of Co and Pd,[33] as observed in the irradiated metallic Co/Pd superlattice. Though further studies are required to understand the effect of hydrogenation of Co/Pd, we believe that the hydrogenation of the Co and Pd atoms does not significantly affect the nanoscale patterning by reduction with low-energy proton irradiation.

TABLE 1. PMA, M_s, and H_C of the Metallic, Irradiated Metallic, and Reduced Metallic Superlattices

superlattice structure	PMA (erg/cm^3)	M_s (emu/cm^3)	H_c (Oe)
$[Co\ 0.4/Pd\ 1.0]_{10}$ (nm)	2.86×10^6	400	500
Irradiated $[Co\ 0.4/Pd\ 1.0]_{10}$ (nm)	2.54×10^6	340	500
[Co (reduced from Co_3O_4) 0.5/Pd 1.0]$_{10}$ (nm)	3.78×10^6	320	2000

We prepared a separate specimen only for the investigation of the crystalline structure of the patterned Co_3O_4/Pd superlattice by cross-sectional high resolution transmission electron microscopy (TEM) because the Co_3O_4 layer was too thin to observe the crystalline structure of the reduced metallic Co layer. The Co_3O_4 thickness was increased from 0.6 to 1.5 nm. We also lowered the number of repetitions of [Co_3O_4/Pd] from 10 to 4 to keep the total film thickness the same and further decreased the pattern size down to 100 nm. An Al layer of ~70 nm was additionally deposited after patterning, to distinguish the photoresist mask from the amorphous carbon layer (the protection layer for FIB) since the mask and carbon layer have similar contrast in the TEM image. The photoresist mask and the unmasked (or window) regions after irradiation are shown in Figure 2. The fast Fourier transformed (FFT) diffraction patterns from the unirradiated area of the superlattice under the mask show a Co_3O_4 (111) plane while those without mask show the absence of Co_3O_4 (111), indicating that the proton-irradiated area is reduced to an FCC Co/Pd (111) metallic phase. The interplanar distance of the Co_3O_4 (111) plane estimated from the diffraction pattern is ~4.6 Å consistent with that from our X-ray diffraction study (not shown). Figure 2 also confirms that the

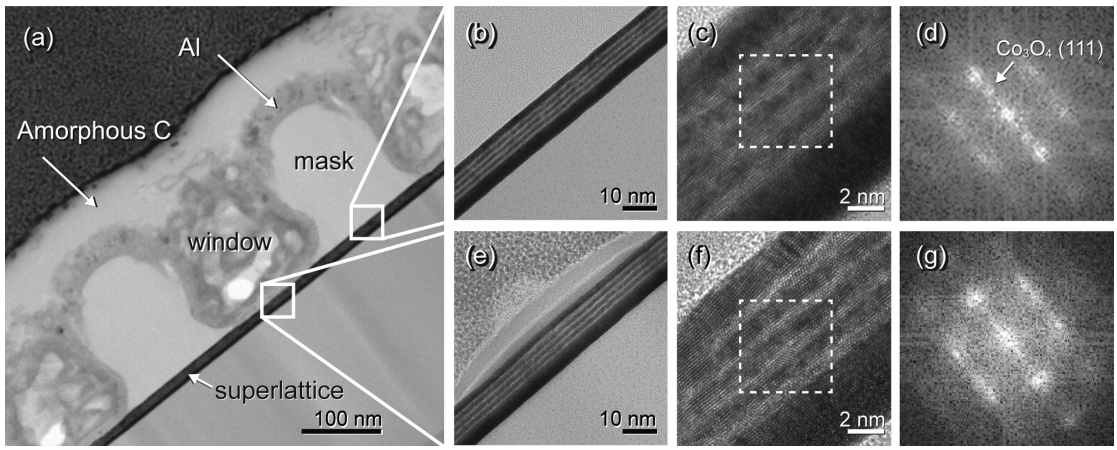

Figure 2. (a) Cross section of the patterned superlattice with the resist mask. High-resolution TEM images of the superlattice under mask (b and c), and under window (e and f). (d and g) The diffraction patterns of the superlattice under the mask and the window, respectively.

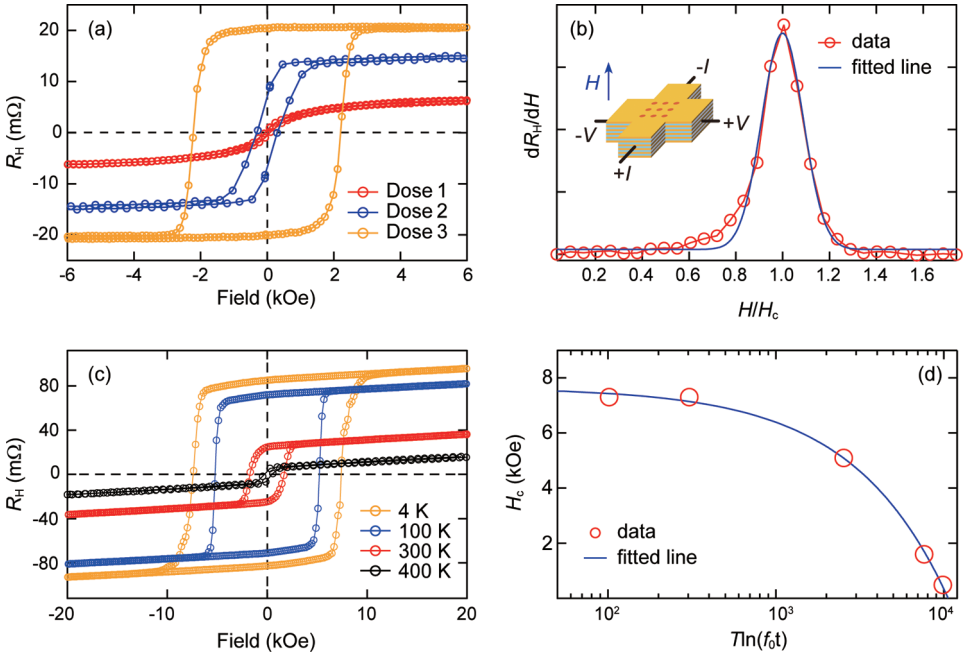

Figure 3. (a) AHE curves of the array of 100 nm-sized islands irradiated at various proton doses. (b) The differential AHE curve of the array patterned at Dose 3 (1.48×10^{17} ions/cm^2). The blue line is the fitted line, and the inset indicates the schematic image of the Hall magnetometry. (c) AHE curves of the array at Dose 3 as a function of temperature *T*. (d) Plots of temperature-dependent coercivity of the array at Dose 3. The plots were fitted using the Sharrock formula (red line).

interfaces between the reduced Co and the Pd layers were still intact and well preserved after patterning. Neither significant damages nor side effects at interfaces were observed.

The dose dependence on the recovery of magnetization in the patterns suggests that a threshold proton dose is required to achieve ferromagnetic transformation. In other words, the patterns remain paramagnetic below the threshold dose. Figure 3a shows the collection of anomalous Hall effect (AHE) curves for 100 nm-sized nanoislands irradiated at a proton dose of 2.97×10^{16} (hereafter called Dose 1), 7.21×10^{16} (Dose 2), and 1.48×10^{17} ions/cm^2 (Dose 3) on which the Hall cross bar was fabricated. The increases in the squareness—the ratio of remanent magnetization to saturation magnetization—and in the change in Hall resistance (ΔR_H) agree well with the ion dose. The fact that the ΔR_H is linearly proportional to magnetic moment[34] suggests that further reduction occurred as the proton dose increased, which increased the magnetic moment of the nanoisland array. The array at Dose 3 showed a squareness of unity, implying that the ferromagnetic nanoislands or the nanomagnets exist as a single ferromagnetic domain in their remanent state. On the other hand, the arrays at Doses 1 and 2 showed a squareness of 0 and 0.25, respectively. Both the small squareness and ΔR_H denote that the Co oxides in the patterns were not fully reduced and

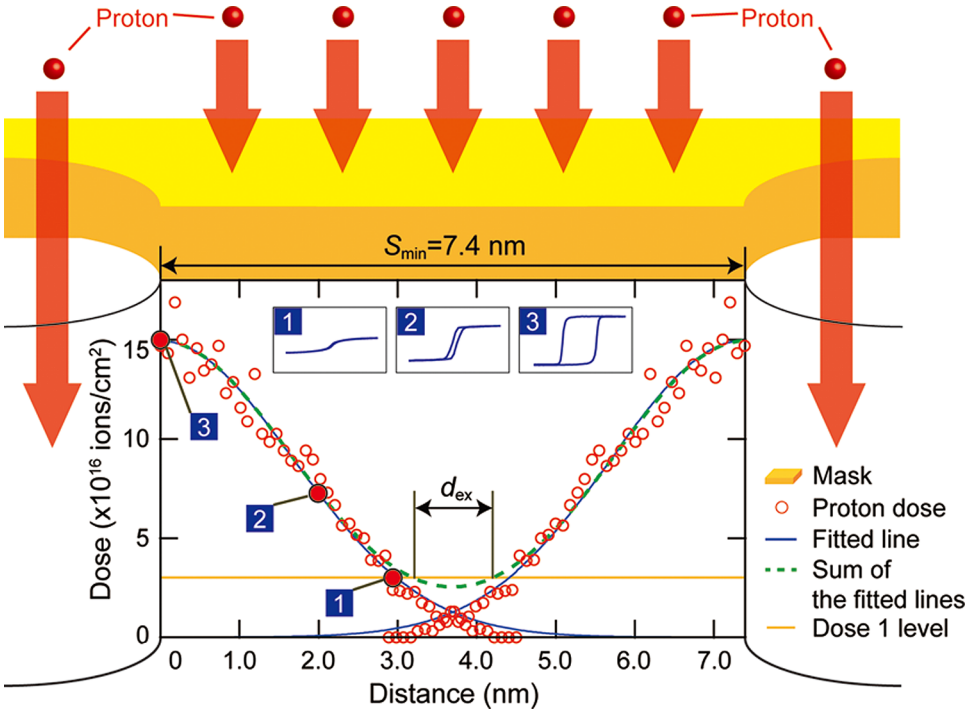

Figure 4. Lateral distributions of the proton dose as a function of a distance from mask edges at Dose 3 (1.48×10^{17} ions/cm^2) with an acceleration energy of 0.5 keV. The numbers 1−3 in blue squares indicate the proton Doses 1−3 and they correspond to those shown in Figure 3a. The loops in the insets with the numbers in blue squares are the schematic hysteresis curves of the patterned nanoislands at each of the doses. The blue lines and the dotted lines are the fitted lines of the distributions and the sum of the fitted lines, respectively. The yellow line indicates Dose 1, which guarantees paramagnetism.

therefore did not induce interfacial PMA.[35−37] In particular, the nanoislands stayed in a paramagnetic state at Dose 1. In our superlattice, the threshold dose lies between Dose 1 and 2, which is crucial to know when one determines the patterning resolution of the proton-irradiation method, as discussed below.

Our proton-irradiated nanoisland array is highly attractive for applications because it (1) has a squareness of unity, (2) exhibits no significant degradation of the intrinsic magnetic anisotropy (K_u) after patterning, and (3) has superior switching field distribution (SFD). A squareness of unity can imply the absence of an edge domain in ferromagnetic islands. The edges of individual islands are the most susceptible to be damaged during the patterning process and they creates a magnetic domain, the so-called edge domain, that is often uncontrollable to switch and difficult to saturate, resulting in the deterioration of squareness and SFD.[38] The K_u is also often significantly reduced due to sidewall damage during conventional fabrication.[38,39] The K_u of the nanoislands was calculated by the generalized Sucksmith-Thompson (GST) method (Supporting Information), which adapts the Hall measurement. We found that $K_1 = K_1^{eff} + 2\pi M_s^2 = 2.95 \times 10^6$ erg/cm^3 and $K_2 = 4.48 \times 10^5$ erg/cm^3. Then, K_u, the sum of K_1 and K_2, becomes 3.40×10^6 erg/cm^3. This value is comparable to that of a continuous film of the reduced superlattice. Therefore, the great advantage of our proton irradiation is that it can transfer the nanoscale patterns without significant side-wall damage. The normalized SFD σ/H_c of the nanomagnet array at Dose 3 was estimated by fitting the derivative of the hysteresis curve with a Gaussian distribution function, as shown in Figure 3 b. The coercivity (H_c) and the standard deviation (σ) were obtained from the fitting. The SFD was ~8%, which is sufficiently small to ensure that each pattern has reliable switching without creating strong pinning centers of domain-walls or disturbing the neighbor patterns.[40] In fact, our proton-irradiated nanoisland array showed SFD superior to that of the nanomagnet array of the Co/Pd superlattice fabricated by a conventional patterning technique.[41−43]

The array of the ferromagnetic island was thermally stable enough to overcome the so-called superparamagnetic limit. By fitting the absolute temperature (T)-dependent H_c plots using the Sharrock's formula,[44] as shown in Figure 3c,d, we found that the thermal stability factor of K_uV/k_BT is ~83 for our reduced nanomagnets at Dose 3, where V and k_B are the nucleation volume and the Boltzmann constant, respectively. The thermal stability of the nanomagnets is strong enough to ensure their magnetic information will last more than 10 years. The lateral size of an individual nanoisland can be shrunk down to 8.2 ± 0.3 nm with a K_u of 3.40×10^6 erg/cm^3 and the thermal stability factor remaining at 83, which satisfies the industrial requirements for BPM.

We corroborated the high magnetic recording density achievable with our low-energy proton irradiation by simulation using SRIM. From the simulation, we confirmed that the proton dose in a lateral straggling showed the Gaussian distribution when the oxidic superlattice was irradiated at Dose 3 (1.48×10^{17} ions/cm^2) with 0.5 keV, as shown in Figure 4. Therefore, protons scattered from the nearest unmasked region cannot be ignored, and their distribution should be counted for estimating the minimum pitch (center-to-center distance between the two nanoislands) in the array. Remember that if the irradiation dose is not higher than Dose 1, paramagnetism is sustained in the superlattice. Considering the overlap of the straggling from the nearest-neighbor mask edge, as shown in Figure 4, we can find the maximum overlapped range where the total dose is lower than Dose 1, and hence paramagnetism is guaranteed to suppress interactions between nanoislands.[45,46] In addition, the distance of quantum mechanical exchange interaction d_{ex} (~1 nm) was considered between ferromagnetic nanoislands for the estimation.[46] Consequently, the minimum edge-to-edge separation (S_{min}) was 7.4 ± 0.2 nm in the case of the proton irradiation energy of 0.5 keV. These results show that the low-energy proton irradiation can provide an array of nanoislands with a pitch of ~15 nm and a critical dimension of less than ~8 nm. This signifies a capability of ~3 Tb/in^2 in magnetic recording.

CONCLUSIONS

To conclude, ferromagnetic nanoislands in a paramagnetic medium were successfully patterned by a local phase transformation with low-energy, nondestructive proton irradiation without significant defects or side effects being generated. Those nanoislands showed attributes capable of a magnetic recording density of 3 Tb/in.^{2} with a thermal stability factor high enough to overcome the superparamagnetic limit. We are currently applying our proton irradiation for patterning of a magnetic and oxidic system, but because unlike other irradiation methods, the basic principle of our nanopatterning is to use a local phase transformation, our method should also be capable of patterning devices composed of other materials systems, including nitrides and sulfides, on a nanometer scale for electronic and optical applications.

METHODS

We prepared a paramagnetic Co_3O_4/Pd superlattice on a Si (100)/SiO_2 200 nm (thermally oxidized) substrate using an ultrahigh vacuum (UHV) DC magnetron sputterer. The structure of the superlattice was Ta 4.0/Pd 3.0/$[Co_3O_4$ 0.6/Pd 1.0$]_{10}$/Pd 2.0 (nm). The base pressure was less than 4.0×10^{-9} Torr. Proton plasma was generated at a working pressure of 1×10^{-2} Torr using microwave power at 2.5 GHz, and the protons were then accelerated to a voltage of 0.5 kV and irradiated onto nanohole array patterns on the Co_3O_4/Pd superlattice. Pattern images were obtained using MFM, and SPEM on the 8A1 beamline at the synchrotron light source of the Pohang Accelerator Laboratory. TEM specimen of the patterned superlattice was separately prepared (see below) using a focused ion beam lift-off technique with Ga ions accelerated at 5 kV. We coated the specimen with a 100 nm-thick amorphous carbon layer and tilted it by 1.5° during the final etching to reduce as much as possible physical damage to the crystalline structure by the bombardment of energetic Ga ions. A nanohole array and a Hall cross bar were separately fabricated using electron-beam (e-beam) lithography to pattern the array of nanoislands in a pillar shape and to study the magnetic characteristics of the array.

Conflict of Interest: The authors declare no competing financial interest.

Acknowledgment. We are grateful to Prof. K. H. Yoo, Dr. H.-J. Shin (8A1 beamline PAL), Dr. Y. Park (NNFC), Mr. H. Youn and Mr. C.-Y. Chung (Park system corp.) for their support in observing pattern images and Dr. G. Choi for discussion about magnetic storage media. This research was supported in part by Basic Science Research Program through the National Research Foundation of Korea NRF funded by the Ministry of Education (NRF-2013R1A1A2013745), Pioneer Research Center Program (2013-008914), the Ministry of Science, ICT and Future Planning and the Pohang Accelerator Laboratory (SM-12), XFEL project, Korea, and the Future Semiconductor Device Technology Development Program (10044723) funded By the Ministry of Trade, Industry & Energy and the Korea Semiconductor Research Consortium.

Supporting Information Available: The GST method to calculate PMA of the array of ferromagnetic islands. This material is available free of charge *via* the Internet at http://pubs.acs.org.

REFERENCES AND NOTES

1. Iwai, H. Roadmap for 22 nm and Beyond. *Microelectron. Eng.* **2009**, *86*, 1520–1528.
2. Fontana, R. E., Jr.; Hetzler, S. R.; Decad, G. Technology Roadmap Comparisons for TAPE, HDD, and NAND flash: Implications for Data Storage Applications. *IEEE Trans. Magn.* **2012**, *48*, 1692–1696.
3. Terris, B.; Thomson, T. Nanofabricated and Self-Assembled Magnetic Structures as Data Storage Media. *J. Phys. D: Appl. Phys.* **2005**, *38*, R199.
4. Chappert, C.; Fert, A.; Van Dau, F. N. The Emergence of Spin Electronics in Data Storage. *Nat. Mater.* **2007**, *6*, 813–823.
5. Yang, J. K.; Chen, Y.; Huang, T.; Duan, H.; Thiyagarajah, N.; Hui, H. K.; Leong, S. H.; Ng, V. Fabrication and Characterization of Bit-Patterned Media Beyond 1.5 Tbit/in^2. *Nanotechnology* **2011**, *22*, 385301.
6. Cobas, E.; Friedman, A. L.; van't Erve, O. M.; Robinson, J. T.; Jonker, B. T. Graphene as a Tunnel Barrier: Graphene-based Magnetic Tunnel Junctions. *Nano Lett.* **2012**, *12*, 3000–3004.
7. Ikeda, S.; Miura, K.; Yamamoto, H.; Mizunuma, K.; Gan, H.; Endo, M.; Kanai, S.; Hayakawa, J.; Matsukura, F.; Ohno, H. A Perpendicular-Anisotropy CoFeB−MgO Magnetic Tunnel Junction. *Nat. Mater.* **2010**, *9*, 721–724.
8. Toyli, D. M.; Weis, C. D.; Fuchs, G. D.; Schenkel, T.; Awschalom, D. D. Chip-Scale Nanofabrication of Single Spins and Spin Arrays in Diamond. *Nano Lett.* **2010**, *10*, 3168–3172.
9. Jiang, X.; Thomas, L.; Moriya, R.; Parkin, S. S. Discrete Domain Wall Positioning Due to Pinning in Current Driven Motion along Nanowires. *Nano Lett.* **2010**, *11*, 96–100.
10. Miron, I. M.; Moore, T.; Szambolics, H.; Buda-Prejbeanu, L. D.; Auffret, S.; Rodmacq, B.; Pizzini, S.; Vogel, J.; Bonfim, M.; Schuhl, A. Fast Current-Induced Domain-wall Motion Controlled by the Rashba Effect. *Nat. Mater.* **2011**, *10*, 419–423.

11. Uchida, K.; Takahashi, S.; Harii, K.; Ieda, J.; Koshibae, W.; Ando, K.; Maekawa, S.; Saitoh, E. Observation of the Spin Seebeck Effect. *Nature* **2008**, *455*, 778–781.
12. Valenzuela, S. O.; Tinkham, M. Direct Electronic Measurement of the Spin Hall Effect. *Nature* **2006**, *442*, 176–179.
13. Neumann, A.; Thönnißen, C.; Frauen, A.; Heße, S.; Meyer, A.; Oepen, H. P. Probing the Magnetic Behavior of Single Nanodots. *Nano Lett.* **2013**, *13*, 2199–2203.
14. Chappert, C.; Bernas, H.; Ferré, J.; Kottler, V.; Jamet, J.-P.; Chen, Y.; Cambril, E.; Devolder, T.; Rousseaux, F.; Mathet, V. Planar Patterned Magnetic Media Obtained by Ion Irradiation. *Science* **1998**, *280*, 1919–1922.
15. Fassbender, J.; Ravelosona, D.; Samson, Y. Tailoring Magnetism by Light-Ion Irradiation. *J. Phys. D: Appl. Phys.* **2004**, *37*, R179.
16. Terris, B.; Folks, L.; Weller, D.; Baglin, J.; Kellock, A.; Rothuizen, H.; Vettiger, P. Ion-Beam Patterning of Magnetic Films Using Stencil Masks. *Appl. Phys. Lett.* **1999**, *75*, 403–405.
17. Suharyadi, E.; Kato, T.; Tsunashima, S.; Iwata, S. Magnetic Properties of Patterned Co/Pd Nanostructures by E-beam Lithography and Ga Ion Irradiation. *IEEE Trans. Magn.* **2006**, *42*, 2972–2974.
18. Ajan, A.; Sato, K.; Aoyama, N.; Tanaka, T.; Miyaguchi, Y.; Tsumagari, K.; Morita, T.; Nishihashi, T.; Tanaka, A.; Uzumaki, T. Fabrication, Magnetic, and R/W Properties of Nitrogen-Ion-Implanted Co/Pd and CoCrPt Bit-Patterned Medium. *IEEE Trans. Magn.* **2010**, *46*, 2020–2023.
19. Kato, T.; Iwata, S.; Yamauchi, Y.; Tsunashima, S.; Matsumoto, K.; Morikawa, T.; Ozaki, K. Planar Patterned Media Fabricated by Ion Irradiation into $CrPt_3$ Ordered Alloy Films. *J. Appl. Phys.* **2009**, *105*, 07C117–1.
20. Rettner, C. T.; Anders, S.; Thomson, T.; Albrecht, M.; Ikeda, Y.; Best, M. E.; Terris, B. D. Magnetic Characterization and Recording Properties of Patterned $Co_{70}Cr_{18}Pt_{12}$ Perpendicular Media. *IEEE Trans. Magn.* **2002**, *38*, 1725–1730.
21. Parekh, V.; Smith, D.; Rantschler, J.; Khizroev, S.; Litvinov, D. He^{+} Ion Irradiation Study of Continuous and Patterned Co/Pd Multilayers. *J. Appl. Phys.* **2007**, *101*, 083904–083904−4.
22. Menéndez, E.; Liedke, M. O.; Fassbender, J.; Gemming, T.; Weber, A.; Heyderman, L. J.; Rao, K. V.; Deevi, S. C.; Surinach, S.; Baro, M. D. Magnetic Recording: Advancing into the Future. *Small* **2009**, *5*, 229–234.
23. Kim, S.; Lee, S.; Ko, J.; Son, J.; Kim, M.; Kang, S.; Hong, J. Nanoscale Patterning of Complex Magnetic Nanostructures by Reduction with Low-Energy Protons. *Nat. Nanotechnol.* **2012**, *7*, 567–571.
24. Fassbender, J. Nanopatterning: The Chemical Way to Ion Irradiation. *Nat. Nanotechnol.* **2012**, *7*, 554–555.
25. Thompson, M. W. *Defects and Radiation Damage in Metals*; Cambridge University Press: Cambridge, U.K., 1974; pp 89−95.
26. Broeders, C. H. M.; Konobeyev, A. Y. Defect Production Efficiency in Metals under Neutron Irradiation. *J. Nucl. Mater.* **2004**, *328*, 197–214.
27. Ziegler, J. F.; Ziegler, M. D.; Biersack, J. P. SRIM—The Stopping and Range of Ions in Matter. *Nucl. Instrum. Methods Phys. Res., Sect. B* **2010**, *268*, 1818–1823.
28. Khalid, M.; Esquinazi, P.; Spemann, D.; Anwand, W.; Brauer, G. Hydrogen-Mediated Ferromagnetism in ZnO Single Crystals. *New J. Phys.* **2011**, *13*, 063017.
29. Friedman, A. L.; Chun, H.; Jung, Y. J.; Heiman, D.; Glaser, E. R.; Menon, L. Possible Room-Temperature Ferromagnetism in Hydrogenated Carbon Nanotubes. *Phys. Rev. B* **2010**, *81*, 115461.
30. Munbodh, K.; Perez, F. A.; Keenan, C.; Lederman, D.; Zhernenkov, M.; Fitzsimmons, M. R. Effects of Hydrogen/Deuterium Absorption on the Magnetic Properties of Co/Pd Multilayers. *Phys. Rev. B* **2011**, *83*, 094432.
31. Jamieson, H. C.; Manchester, F. D. The Magnetic Susceptibility of Pd, PdH and PdD between 4 and 300 K. *J. Phys. F: Met. Phys.* **1972**, *92*, 323.
32. Ishimatsu, N.; Shichijo, T.; Matsushima, Y.; Maruyama, H.; Matsuura, Y.; Tsumuraya, T.; Shishidou, T.; Oguchi, T.; Kawamura, N.; Mizumaki, M.; Matsuoka, T.; Takemura, K. Hydrogen-Induced Modification of the Electronic Structure and Magnetic States in Fe, Co, and Ni Monohydrides. *Phys. Rev. B* **2012**, *86*, 104430.
33. Okamoto, S.; Kitakami, O.; Shimada, Y. Enhancement of Magnetic Anisotropy of Hydrogenated Pd/Co/Pd Trilayers. *J. Magn. Magn. Mater.* **2002**, *239*, 313.
34. Webb, B. C.; Schultz, S. Detection of the Magnetization Reversal of Individual Interacting Single-Domain Particles within Co-Cr Columnar Thin-Films. *IEEE Trans. Magn.* **1988**, *24*, 3006–3008.
35. Bruno, P.; Renard, J.-P. Magnetic Surface Anisotropy of Transition Metal Ultrathin Films. *Appl. Phys. A: Mater. Sci. Process.* **1989**, *49*, 499–506.
36. Kyuno, K.; Ha, J.-G.; Yamamoto, R.; Asano, S. Magnetoelastic Contribution to the Interface Anisotropy of Pd/Co Metallic Multilayers. *Phys. Rev. B* **1996**, *54*, 1092.
37. Engel, B. N.; England, C. D.; Van Leeuwen, R. A.; Wiedmann, M. H.; Falco, C. M. Interface Magnetic Anisotropy in Epitaxial Superlattices. *Phys. Rev. lett.* **1991**, *67*, 1910–1913.
38. Shaw, J. M.; Silva, T. J.; Schneider, M. L.; McMichael, R. D. Spin Dynamics and Mode Structure in Nanomagnet Arrays: Effects of Size and Thickness on Linewidth and Damping. *Phys. Rev. B* **2009**, *79*, 184404.
39. Shaw, J. M.; Russek, S. E.; Thomson, T.; Donahue, M. J.; Terris, B. D.; Hellwig, O.; Dobisz, E.; Schneider, M. L. Reversal Mechanisms in Perpendicularly Magnetized Nanostructures. *Phys. Rev. B* **2008**, *78*, 024414.
40. Ranjbar, M.; Piramanayagam, S.; Suzi, D.; Aung, K. O.; Sbiaa, R.; Kay, Y. S.; Wong, S. K.; Chong, C. T. Antiferromagnetically Coupled Patterned Media and Control of Switching Field Distribution. *IEEE Trans. Magn.* **2010**, *46*, 1787–1790.
41. Thomson, T.; Hu, G.; Terris, B. D. Intrinsic Distribution of Magnetic Anisotropy in Thin Films Probed by Patterned Nanostructures. *Phys. Rev. Lett.* **2006**, *96*, 257204.
42. Hellwig, O.; Berger, A.; Thomson, T.; Dobisz, E.; Bandic, Z. Z.; Yang, H.; Kercher, D. S.; Fullerton, E. E. Separating Dipolar Broadening from the Intrinsic Switching Field Distribution in Perpendicular Patterned Media. *Appl. Phys. Lett.* **2007**, *90*, 162516.
43. Shaw, J. M.; Rippard, W. H.; Russek, S. E.; Reith, T.; Falco, C. M. Origins of Switching Field Distributions in Perpendicular Magnetic Nanodot Arrays. *J. Appl. Phys.* **2007**, *101*, 023909.
44. Brown, C. S.; Harrell, J. W.; Matsunuma, S. Time and Temperature Dependences of the Magnetization Reversal in a Co/Pd Multilayer Film. *J. Appl. Phys.* **2006**, *100*, 053910.
45. Johnson, K. E. Magnetic Materials and Structures for Thin-Film Recording Media. *J. Appl. Phys.* **2000**, *87*, 5365.
46. Guimarães, A. P. *Principles of Nanomagnetism*; Springer: Germany, 2009; p 4.